Impact of AlN interlayer on the electronic and I-V characteristics of $In_{0.17}Al_{0.83}N$/GaN HEMTs devices

A. Douara
Faculty of Science and Technology, Tissemsilt University, Algeria.

A. Rabehi
Laboratoire de Micro-électronique Appliquée. Université Djillali Liabès de Sidi Bel Abbés, BP 89, 22000, Sidi Bel Abbés, Algeria,
Faculty of Science and Technology, Ziane Achour University of Djelfa, Djelfa, Algeria.

O. Baitiche
Laboratory of Semi-conductors and Functional materials, Ammar Thlidji University of Laghouat, Algeria.

Received 1 September 2022; accepted 29 November 2022

Here, we study a simulation model of $In_{0.17}Al_{0.83}N$/GaN passivated high electron mobility transistors (HEMTs) on SiC substrate. The research focused systematically on the effect of AlN interlayer on the electronic and electric characteristics. The 2D-electron gas density of $In_{0.17}Al_{0.83}N$/AlN/GaN HEMTs is investigated through the dependence on various AlN layer thickness. We report calculations of I-V characteristics, with 1.5 nm AlN thickness. We find the highest maximum output current of 1.81 A/mm at Vgs = 1 V, and more than 450 mS/mm as a transconductance peak. The Results are in agreement with experimental data.

Keywords: HEMTs; AlN interlayer; 2D-electron gas.

DOI: https://doi.org/10.31349/RevMexFis.69.031602

1. Introduction

Compound materials from group III-N achieved significant progress in optoelectronic devices for a broad range of applications [1–6]. The AlGaN/GaN HEMTs have been successfully used for high power, high speed and high temperature operations [7, 8], because its properties are consistent for high frequency and power that allow obtaining extremely high power densities in RF HEMT [9]. However, by switching the AlGaN barrier layer with InAlN, the device performance may still be improved [10].

Recently, it has been proven that InAlN transistors have good performance for applications in power device applications due to its strong piezoelectric effect at the interface [11]. Meanwhile, the sheet concentration in the channel of 10^{13} cm^{-2} by the difference in spontaneous polarization is larger than the other HEMTs devices based of III-V [12, 13].

The electron sheet density of 1.9×10^{13} cm^{-2} in the proposed device [14] with 30 nm T-shaped gate length has been obtained with SiC substrates, and a maximum oscillation frequency of 340 GHz. At Vgs = 1 V, the maximum drain saturation current density of 1.65 A/mm has been reported in 70 nm gate length $In_{0.17}Al_{0.83}N$/AlN/GaN HEMT with a 1 nm AlN spacer layer thickness [15], and the peak transconductance above of 380 mS/mm. The device [16] has a 13 nm thick AlInN barrier layer containing 81% Al. Hall-Effect measurements at 77 K give a sheet carrier density of 2.5×10^{13} cm^{-2}.

The proposed model of $In_{0.17}Al_{0.83}N$/AlN/GaN heterostructures was improved. In this work we investigate the impact of spacer layer (AlN) thickness on the electronic properties and current-voltage characteristics using the nextnano simulator [17]. The analysis of the 2DEG interface charge density was accomplished by a self-consistent solution of Schrödinger and Poisson equations. The energy eigenvalues and eigenvectors are obtained by self-consistently solving these equations.

2. Self-consistently model for 2D-electron gas interface charge density

Table I illustrate the standard definitions of used symbols. By finite difference method (FDM) we solve the Schrödinger and Poisson equations self-consistently and derive the conduction band, and wave-function of 2DEG in the channel [18]. The Schrödinger equation is [19]:

$$-\frac{\hbar^2}{2}.\frac{d}{dz}.\left(\frac{1}{m^*(z)}.\frac{d}{dz}\right)\psi(z)+V(z)\psi(z)=E\psi(z). \quad (1)$$

The Poisson's equation in one dimension is [20]:

$$\frac{d}{dz}\left(\varepsilon_s(z)\frac{d}{dz}\right)\varphi(z)=-\frac{\rho(z)}{\varepsilon_0}=\frac{-q[N_D(z)-n(z)]}{\varepsilon_0}. \quad (2)$$

The potential energy expressed [21, 22]:

$$V(z)=-q\varphi(z)+\Delta E_c(z), \quad (3)$$

TABLE I. List of symbols.

Symbol	Description
ψ	Wave function
E	The energy
φ	The electrostatic potential
m^*	The effective mass
ε_s	The dielectric constant
$\hbar$	Planck's constant divided by 2π
$n(z)$	The electron density distribution
σ	The sheet charge density at the interface
ΔE_c	The conduction band discontinuity
E_k	The Eigenenergy of the k-th state
$N_D(z)$	The ionized donor concentration
n_k	The electron occupation at k-th state
ε_{AlInN}	The dielectric constants of AlInN barrier
ε_{GaN}	The dielectric constants of GaN channel
P_{sp}	The spontaneous polarization
$e_{31},\ e_{33}$	Piezoelectric constants
$C_{13},\ C_{33}$	Elastic constants
$a(0),\ a(x)$	The values of lattice constant
μ_n	The drift mobility of electron
W	The width of channel layer
V_{th}	The threshold voltage

where $\psi(z)$ and $n(z)$ are related by [23]:

$$n(z) = \sum_{k=1}^{n} \psi_k^*(z)\psi_k(z)n_k. \tag{4}$$

For each state, the electron density can be described by [24]:

$$n_k = \frac{m^*}{\pi\hbar^2}\int_{E_k}^{\infty} \frac{1}{1+e^{(E-E_f)/kT}}dE \tag{5}$$

$$= \frac{m^* kT}{\pi\hbar^2}\ln\left(1+\exp\left[\frac{E_f-E_k}{kT}\right]\right). \tag{6}$$

Polarization sheet charge can be deduced at interface of InAlN/GaN by [21]:

$$E_{\text{AlInN}}\varepsilon_{\text{AlInN}} - E_{\text{GaN}}\varepsilon_{\text{GaN}} = -\sigma, \tag{7}$$

and σ is given by the following relationship [21]:

$$\sigma(y) = 2\frac{a(0)-a(x)}{a(x)}\left(e_{31}(x) - e_{33}(x)\frac{C_{13}(x)}{C_{33}(x)}\right) + \left(P_{sp}(x) - P_{sp}(0)\right). \tag{8}$$

It can be expressed spontaneous polarization by [25]:

$$P_{sp(\text{In}_x\text{Al}_{1-x}\text{N})} = -0.09x - 0.042(1-x) + 0.07x(1-x)\ \text{C/m}^2. \tag{9}$$

The current drain-source is given by [26]:

$$I_{DS} = W\mu_n q n_s E. \tag{10}$$

As the current is constant in the channel, Eq. (9) can be integrated from drain-source [27]:

$$I_{DS} = \frac{W\mu_n C_0}{L}\left(\left[V_{GS}-V_{th}\right]V_{DS} - \frac{V_{DS}^2}{2}\right), \tag{11}$$

where V_{DS} is much lower than $(V_{GS}-V_{th})$, the Eq. (10) becomes [28]:

$$I_{\text{lin}} = (W\mu_n C_0(V_{GS}-V_{th})V_{DS})/L. \tag{12}$$

The current of drain -source saturation is given by [27]:

$$I_{DS.sat} = \frac{W\mu_n C_0}{2L}(V_{GS}-V_{th})^2. \tag{13}$$

As we know that these equations are difficult to solve analytically, we used the nextnano device simulation software [16].

3. Device structure

The cross sectional view of $In_{0.17}Al_{0.83}N$/GaN device is depicted in Fig. 1, our device is grown on an insulating Silicon carbide substrate (SiC), a 2 μm undoped GaN semi-insulating layer, and an AlN spacer layer with various thickness (d), and basically composed of an 8 nm undoped InAlN barrier layer, the device structures are T-shaped passivated with SiN recessed gate length of 70 nm.

Finally, the source-drain spacing is 2 μm. In our calculations, the AlN thickness is used as a parameter. The 2-DEG is formed at the heterointerface of $In_{0.17}Al_{0.83}N$/GaN as shown in Fig. 1.

4. Results and discussions

Figure 2 displays the calculated band diagram, and wavefunction of 2DEG in the channel of $In_{0.17}Al_{0.83}N$/GaN HEMT structures without and with a 1 nm AlN spacer, under zero applied voltage.

We found that the sheet carrier density in the 2-D electron gas is in the order of 10^{19} cm^{-3}. It was observed enhanced electron confinement with AlN spacer layer. The height of a potential barrier affects how the wave function penetrates the barrier layer. The AlN spacer significantly increases the barrier height and therefore suppresses this effect, due to the fact that AlGaN is a ternary material.

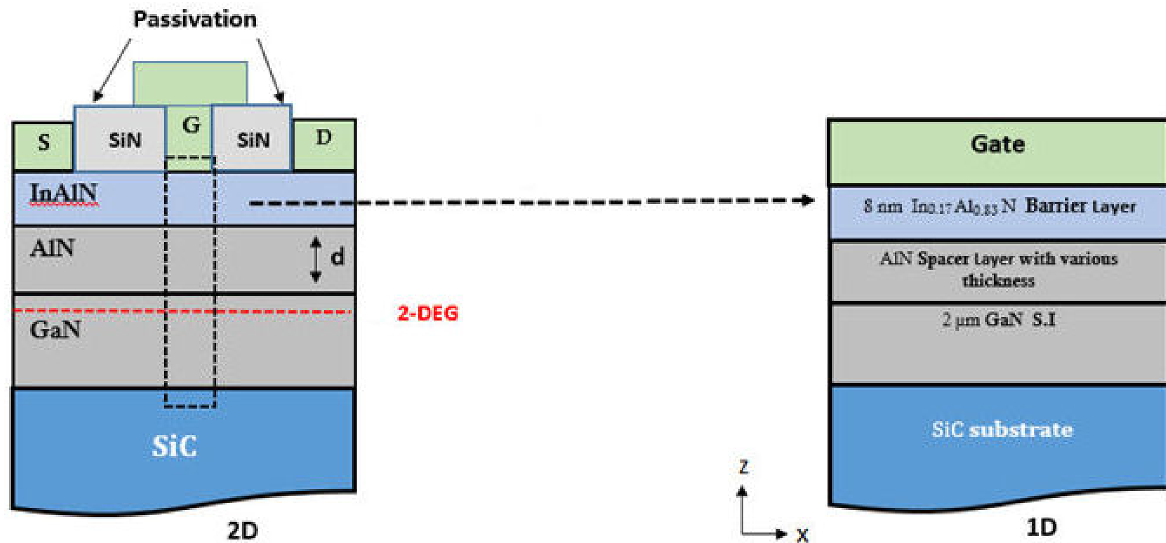

FIGURE 1. The schematic structure of InAlN/GaN device studied.

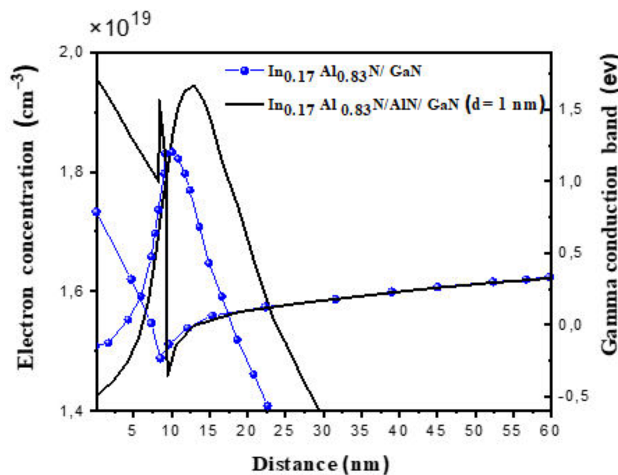

FIGURE 2. Electron density (ns) and gamma conduction band energy (E_c) of $\mathrm{In_{0.17}Al_{0.83}N/GaN}$ HEMTs with and without an AlN spacer layer.

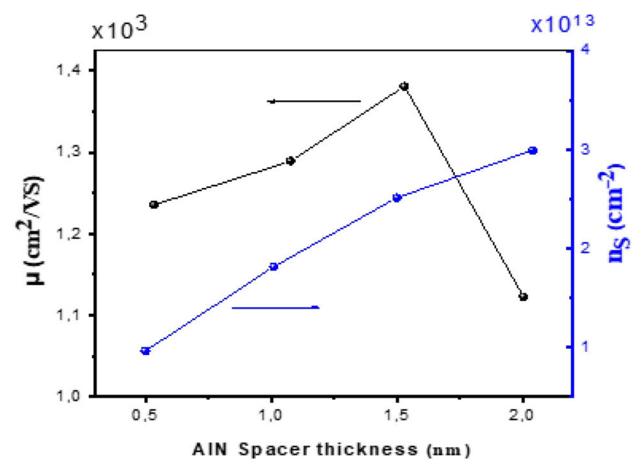

FIGURE 3. Mobility and sheet carrier concentration (ns) of 2D - electron gas (2DEG)Vs AlN spacer layer thickness.

4.1. Sheet carrier concentration (n_s)

The variation of the 2D-electron gas density for different AlN spacer layer thicknesses is shown in Fig. 3. The higher the spacer layer thickness the better the sheet charge density (ns), with an almost linear dependence on the AlN spacer layer thickness range between 0.5 nm and 2 nm. The increase in electron density is due to the effect of piezoelectric and spontaneous polarization.

Due to the significant polarization effect, the AlN spacer may cause an increase in dipole scattering and, as a result, the 2-D electron gas mobility will decline. Spacer enhances conduction band shift below this critical thickness, which effectively reduces the penetration of the wave function into the AlN barrier and thus reduces the effect of alloy disorder diffusion. The electron sheet density of 1.81×10^{13} cm^{-2} is roughly similar to that calculated in [15] for 1 nm AlN layer.

Also in Fig. 3, we found that the electron mobility increases while increase the AlN interlayer thickness.

For 1.5 nm AlN, we observe the highest mobility (1380 cm^2/V.s) for this structure, the sheet carrier concentration reached 2.5×10^{13} cm^{-2}. Also, we see the electron mobility of 1253 cm^{-2}/V.s, which is very similar to those obtained by Tingting *et al.* [15].

4.2. Transfer characteristics

Figure 4a) illustrates the transfer characteristics of $\mathrm{In_{0.17}Al_{0.83}N/GaN}$ HEMT for $V_{DS} = 7$ V.

The thickness of the AlN spacer layer increased from 0.5 nm to 2 nm. It is reported here that the drain current increases by increasing the AlN thickness. The maximum drain-source current for 1.5 nm AlN is 1.81 A/mm due to the increase of the mobility with spacer layer and 2D-electron gas density, while it decreases to 0.82 A/mm for $d = 2$ nm due to the mobility degradation.

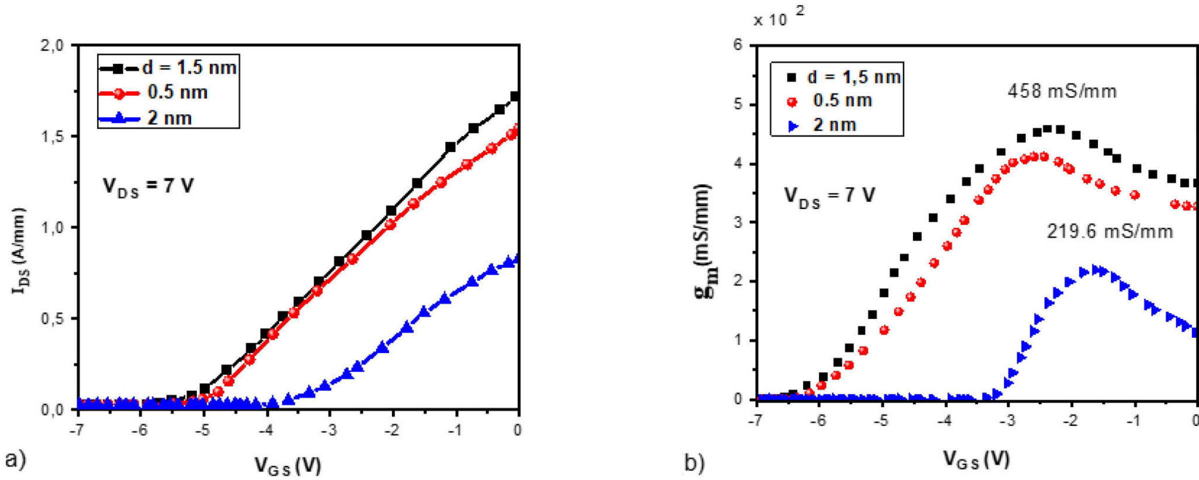

FIGURE 4. Transfer characteristics of $In_{0.17}Al_{0.83}N$/AlN/GaN HEMTs for different AlN spacer layer thickness values. a) I_{DS} as a function of V_{GS}, b) g_m as a function of V_{GS}.

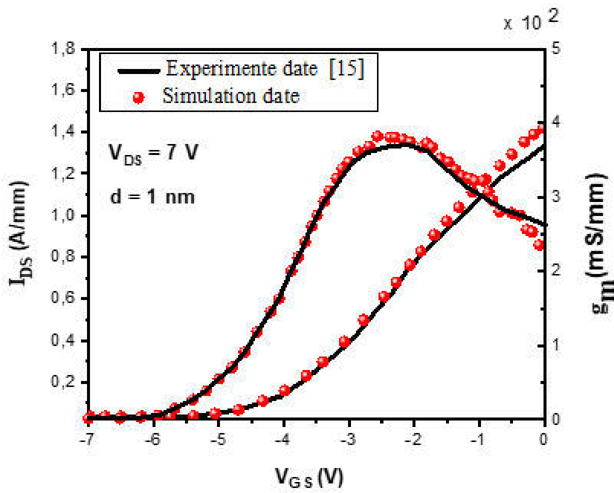

FIGURE 5. Comparison between the results of simulations and experimental [15] transfer characteristics of $In_{0.17}Al_{0.83}N$/AlN/GaN HEMTs at $V_{DS} = 7$ V.

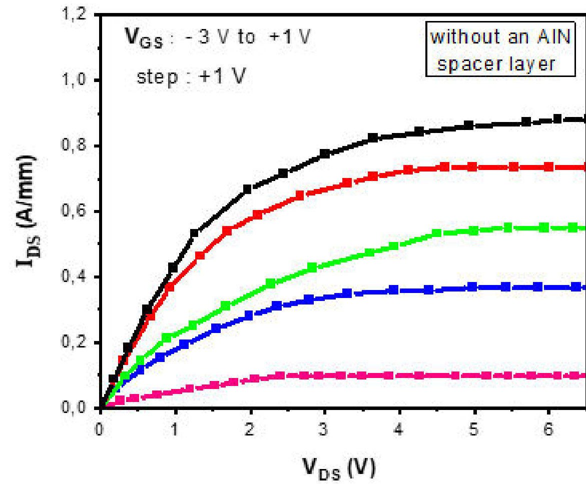

FIGURE 6. Drain characteristics of $In_{0.17}Al_{0.83}N$/GaN HEMTs without an AlN spacer layer. The gate-source voltage is stepped in +1 V steps from -3 V to 1 V.

We have determined the transconductance at each bias (V_{GS}) as in the relationship below:

$$g_m = \frac{\partial I_{DS}}{\partial V_{GS}} | V_{DS} = \text{constant}. \qquad (14)$$

The transconductance's bias dependent on V_{GS} at $V_{DS} = 7$ V is shown in Fig. 4b) for different thicknesses of the AlN spacer layer.

All the device's maximums of transconductance ($g_{m.\max}$) are in the range of $219 - 460$ mS/mm. With the decrease of the AlN thickness, beyond 1.5 nm, we observe that $g_{m.\max}$ decrease from 458 mS/mm for 1.5 nm AlN layer to 219.6 mS/mm for 2 nm owing to the significant decay in the scattering of 2D- electron gas.

The simulated transfer characteristics (Fig. 5) with a 1 nm AlN interlayer show good agreement with the previously reported experimental results [15].

4.3. Output characteristics

Figure 6 illustrates the simulated drain current (I_{DS}) versus gate voltage (V_{DS}) for different values of gate-source voltage (V_{GS}) of $In_{0.17}Al_{0.83}N$/GaN HEMTs without AlN spacer layer.

When the gate-to-source voltage changed from -3 V to 1 V, with the gate biased equal to 1 V , the maximum drain saturation current density was found to be 0.96 A/mm, this significant drain current is due to effects of the strong polarization in $In_{0.17}Al_{0.83}N$/GaN barrier layer, and the InAlN/GaN interface reached with (2DEG) sheet carrier density. Also, the short distance of drain-source plays an essential role because it reduces the parasitic resistance.

The characteristics with a 0.5 nm AlN spacer layer are illustrated in Fig. 7. The highest value of drain current density was 1.48 A/mm (at $V_{GS} = +1$ V).

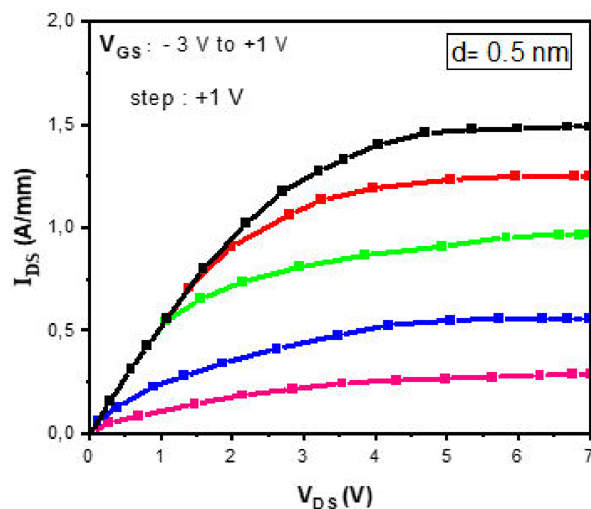

FIGURE 7. Drain characteristics of $In_{0.17}Al_{0.83}N$/GaN HEMTs with 0.5 nm spacer layer. The gate-source voltage is stepped in +1 V steps from -3 V to 1 V.

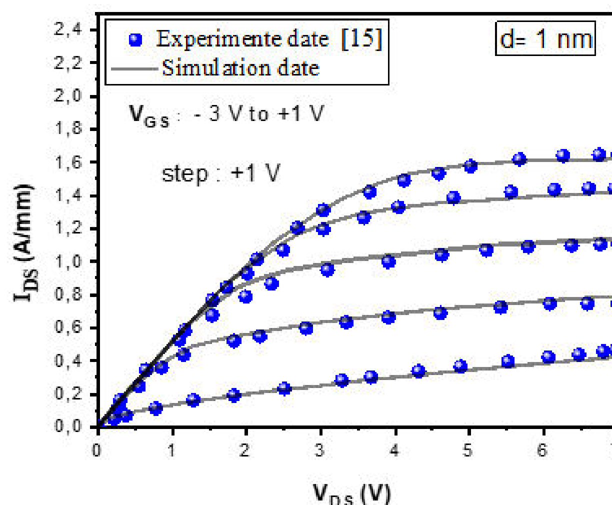

FIGURE 9. Comparison of experimental (symbols) [15] with simulated data of output characteristics of $In_{0.17}Al_{0.83}N$/GaN HEMTs.

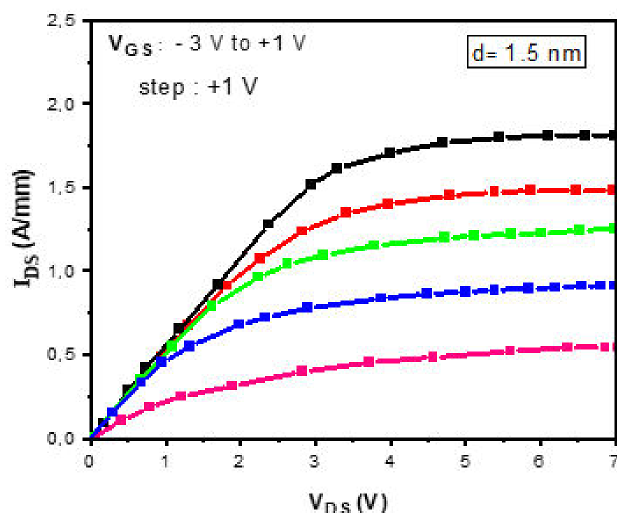

FIGURE 8. Drain characteristics of $In_{0.17}Al_{0.83}N$/GaN HEMTs with 1.5 nm spacer layer. The gate-source voltage is stepped in +1 V steps from -3 V to 1 V.

As seen from Fig. 8, for 1.5 nm AlN, we find that saturated drain current density was 1.81 A/mm, which reflects the high electron density in this newly proposed structure owed to AlN material that holds the highest spontaneous polarization among all III-N.

With a 1 nm AlN spacer layer, we also report an excellent agreement between experimental data [15] and simulation results (see Fig. 9).

5. Conclusion

In summary, we have studied the electronic and electric properties of InAlN/GaN HEMT. We find that a very high electron charge density can be produced due to the strong piezoelectric effect at the interface. The electron density increases with the increase of the AlN thickness.

The increase in electron density is mainly due to the higher piezoelectric charge. Furthermore, we observed that with the optimum thickness (1.5 nm) of the AlN spacer for the $In_{0.17}Al_{0.83}N$/GaN device, the electron density extremely raises close to 2.5×10^{13} cm^{-2}, allowing an electron mobility considerably over of 1350 cm^2/V.s.

The simulations results find an excellent agreement with the experimental data.

1. A. Kacha *et al.*, Effects of the GaN layers and the annealing on the electrical properties in the Schottky diodes based on nitrated GaAs, *Superlattices and Microstructures* **83** (2015) 827, https://doi.org/10.1016/j.spmi.2015.04.017.

2. Rabehi, Abdelaziz *et al.*, Study of the characteristics currentvoltage and capacitance-voltage in nitride GaAs Schottky diode, *Eur. Phys. J. Appl. Phys.* **72** (2015) 10102, https://doi.org/10.1051/epjap/2015150140.

3. Y. Zhang *et al.*, III-V nanowires and nanowire optoelectronic devices, *Journal of Physics D: Applied Physics* **48** (2015) 463001, https://doi.org/10.1088/0022-3727/48/46/463001.

4. A. Rabehi *et al.*, Electrical and photoelectrical characteristics of Au/GaN/GaAs Schottky diode, *Optik* **127** (2016) 6412, https://doi.org/10.1016/j.ijleo.2016.04.113.

5. A. Rabehi *et al.*, Simulation and experimental studies of illumi-

nation effects on the current transport of nitridated GaAs Schottky diode, *Semiconductors* **52** (2018) 1998, https://doi.org/10.1134/S106378261816025X.

6. H. Helal *et al.*, Comparative study of ionic bombardment and heat treatment on the electrical behavior of Au/GaN/n-GaAs Schottky diodes, *Superlattices and Microstructures* **135** (2019) 106276, https://doi.org/10.1016/j.spmi.2019.106276.
7. A. Douara, N. Kermas, and B. Djellouli, Capacitance Models of AlGaN/GaN High Electron Mobility Transistors, *International Journal of Nuclear and Quantum Engineering* **10** (2016) 420, https://doi.org/10.5281/zenodo.1123731.
8. K. Narang *et al.*, Suitability of thin-GaN for AlGaN/GaN HEMT material and device, *Journal of Materials Science* **57** (2022) 5913, https://doi.org/10.1007/s10853-022-07017-x.
9. A. A. Fletcher and D. Nirmal, A survey of Gallium Nitride HEMT for RF and high power applications, *Superlattices and Microstructures* **109** (2017) 519, https://doi.org/10.1016/j.spmi.2017.05.042.
10. J. Ren *et al.*, Comparison of electrical characteristics between AlGaN/GaN and lattice-matched InAlN/GaN heterostructure Schottky barrier diodes, *Microelectronics Reliability* **61** (2016) 82, https://doi.org/10.1016/j.microrel.2015.11.005.
11. A. Y. Polyakov *et al.*, Trapping Phenomena in InAlN/GaN High Electron Mobility Transistors, *ECS Journal of Solid State Science and Technology* **7** (2018) Q1, https://doi.org/10.1149/2.0131802jss.
12. . Y. Liu *et al.*, The Sensing Mechanism of InAlN/GaN HEMT, *Crystals* **12** (2022) 401, https://doi.org/10.3390/cryst12030401.
13. E. Kohn and F. Medjdoub, InAlN-A new barrier material for GaN-based HEMTs, *In 2007 International Workshop on Physics of Semiconductor Devices* (IEEE, 2007) pp. 311-316. https://doi.org/10.1109/IWPSD.2007.4472506.
14. P. Murugapandiyan, S. Ravimaran, and J. William, 30 nm Tgate enhancement-mode InAlN/AlN/GaN HEMT on SiC substrates for future high power RF applications, *Journal of Semiconductors* **38** (2017) 084001, https://doi.org/10.1088/1674-4926/38/8/084001.
15. T. Han *et al.*, 70-nm-gated InAlN/GaN HEMTs grown on SiC substrate with fT/fmax>160 GHz, *Journal of Semiconductors* **37** (2016) 024007, https://doi.org/10.1088/1674-4926/37/2/024007.
16. F. Medjdoub *et al.*, Can InAlN/GaN be an alternative to high power/high temperature AlGaN/GaN devices?, *In 2006 International Electron Devices Meeting* (IEEE, 2006) pp. 1-4, https://doi.org/10.1109/IEDM.2006.346935.
17. https://www.wsi.tum.de/nextnano3 and https://www.nextnano.de,Accessedon10/12/2022.
18. F. Li, Q. H. Liu, and D. P. Klemer, Numerical Simulation of high electron mobility transistors based on the spectral element Method, *The Applied Computational Electromagnetics Society Journal* (ACES) (2016) 1144, https://journals.riverpublishers.com/index.php/ACES/article/view/9859.
19. L. B. d. Carvalho, W. C. d. Santos, and E. d. A. Correa, Solution of the 1d Schrödinger Equation for a Symmetric Well, *Revista Brasileira de Ensino de Física* **41** (2019), https://doi.org/10.1590/1806-9126-RBEF-2018-0359.
20. A. Acharyya *et al.*, Self-consistent solution of Schrödinger-Poisson equations in a reverse biased nanoscale p-n junction based on Si/Si0.4Ge0.6/Si quantum well, *Journal of Computational Electronics* **14** (2015) 180, https://doi.org/10.1007/s10825-014-0637-1.
21. I.-H. Tan *et al.*, A self-consistent solution of Schrodinger Poisson equations using a nonuniform mesh, *Journal of applied physics* **68** (1990) 4071, https://doi.org/10.1063/1.346245.
22. A. Douara *et al.*, Optimization of two-dimensional electron gas characteristics of AlGaN/GaN high electron mobility transistors, *International Journal of Numerical Modelling: Electronic Networks, Devices and Fields* **32** (2019) e2518, https://doi.org/10.1002/jnm.2518.
23. A. Bag *et al*., 2DEG modulation in double quantum well enhancement mode nitride HEMT, *Physica E: Low-dimensional Systems and Nanostructures* **74** (2015) 59, https://doi.org/10.1016/j.physe.2015.06.011.
24. O. Ambacher *et al*., Polarization induced interface and electron sheet charges of pseudomorphic ScAlN/GaN, GaAlN/GaN, In- AlN/GaN, and InAlN/InN heterostructures, *Journal of Applied Physics* **129** (2021) 204501, https://doi.org/10.1063/5.0049185.
25. T.-C. Han, *et al*., Simulation study of InAlN/GaN high-electron mobility transistor with AlInN back barrier, *Chinese Physics B* **26** (2017) 107301, https://doi.org/10.1088/1674-1056/26/10/107301.
26. D. Bouguenna *et al*., 2D Simulations of Current-voltage Characteristics of Cubic AlxGa1-xN/GaN Modulation Doped Hetero-junction Field Effect Transistor Structures, *Sci. Acad. Pub. Electr. Electron. Eng.* **2** (2012) 309, https://doi.org/10.5923/j.eee.20120205.11.
27. A. Douara *et al.*, 2-D optimisation current-voltage characteristics in AlGaN/GaN HEMTs with influence of passivation layer, *International Journal of Ambient Energy* **42** (2021) 1363, https://doi.org/10.1080/01430750.2019.1608856.
28. A. Douara *et al*., IV Characteristics Model For AlGaN/GaN HEMTs Using Tcad-Silvaco (2015), *Journal of New Technology and Materials* (JNTM) **4** (2014) 1924.